Journal of Microscopy, Vol. 190, Pts 1/2, April/May 1998, pp. 99–108.
Received 10 March 1997; accepted 23 July 1997

Why don't high-resolution simulations and images match?

C. B. BOOTHROYD
Department of Materials Science and Metallurgy, University of Cambridge, Pembroke St., Cambridge CB2 3QZ, U.K.

Key words. Electron microscopy, energy-filtered imaging, high-resolution electron microscopy, image simulation, quantitative microscopy

Summary

Computer simulations have been used for many years to understand experimental high-resolution electron microscope images in a qualitative fashion, but the trend nowadays has been to attempt more quantitative image matching. This has led to the discovery that the contrast in experimental images is much less than in simulated images, typically by a factor of about three. There are many possible causes for this discrepancy, ranging from the mechanisms of scattering of electrons by the specimen through the calculations of the diffracted beam intensities and their focusing by the objective lens to the point spread function of the recording device. No single cause can explain all of the experimental contrast loss, although a combination of many factors could.

Introduction

In the past computer simulations have been very successful in calculating images that match qualitatively experimental high-resolution electron microscope images. As a result, many structures have been matched and interface problems solved (e.g. Cherns *et al.*, 1982; Inkson & Humphreys, 1995; Campbell, 1996). There is now however a fashion for 'quantitative' microscopy, which is in fact not so recent (e.g. Bahr & Zeitler, 1965) but is just part of the general trend to matching images in a more quantitative fashion. Many of the earlier problems involved distinguishing between models that were very distinct from one another and thus produced very different simulated images. Thus it was easy to distinguish the correct from the wrong model by a qualitative comparison of the simulated and experimental images where only the positions and general shape of the 'blobs' were matched. With increasing confidence people have attempted to distinguish more subtle differences in structures, such as the oxygen content of high-temperature superconductors (Hÿtch & Stobbs, 1988). This has necessitated a quantitative match between images and simulations. It has become necessary to compare the image *intensity* (the average value of the image on a scale where the incident intensity is one), the image *contrast* (a measure of the amplitude of the lattice fringes), as well as the image *pattern* (the shape distribution of blobs). Of these the image contrast and pattern are the most useful indicators of a match while the image intensity is an indication of the number of electrons lost as a result of absorption and scattering outside the objective aperture. With such quantitative comparisons it is becoming clear that the contrast in experimental high-resolution images is invariably much less, typically by about a factor of three, than that predicted by image simulations (Hÿtch & Stobbs, 1994; Boothroyd *et al.*, 1995; von Hochmeister & Phillipp, 1996), even when images are energy filtered.

In this paper I will go through the stages in the formation of high-resolution images in the approximate order seen by an electron and consider some of the possible causes for why the contrast is found to be lower experimentally than is predicted by simulations.

Scattering of electrons by the specimen

Crystalline materials diffract electrons to angles of up to a few degrees, and it is this elastic scattering that is modelled in image simulations. In reality, many additional forms of scattering, mostly inelastic (but some elastic, such as diffuse scattering), also occur which are (usually) not modelled by image simulations. This is illustrated by Fig. 1, which shows the scattering as a function of angle and energy loss for a thin amorphous Ge film (Boothroyd *et al.*, 1997). In this figure brightness is proportional to the log of the scattered intensity and additionally two contours are plotted per order of magnitude increase in scattered intensity. Elastic diffraction causes angular scattering but no energy loss and thus such electrons are concentrated in the vertical bright line at the left, the zero-loss peak. The same is true for diffuse scattering caused by the atoms being displaced from their lattice positions as a result of the thermal motion of the individual atoms (I will call this thermal diffuse scattering). Scattering caused by the creation of a phonon

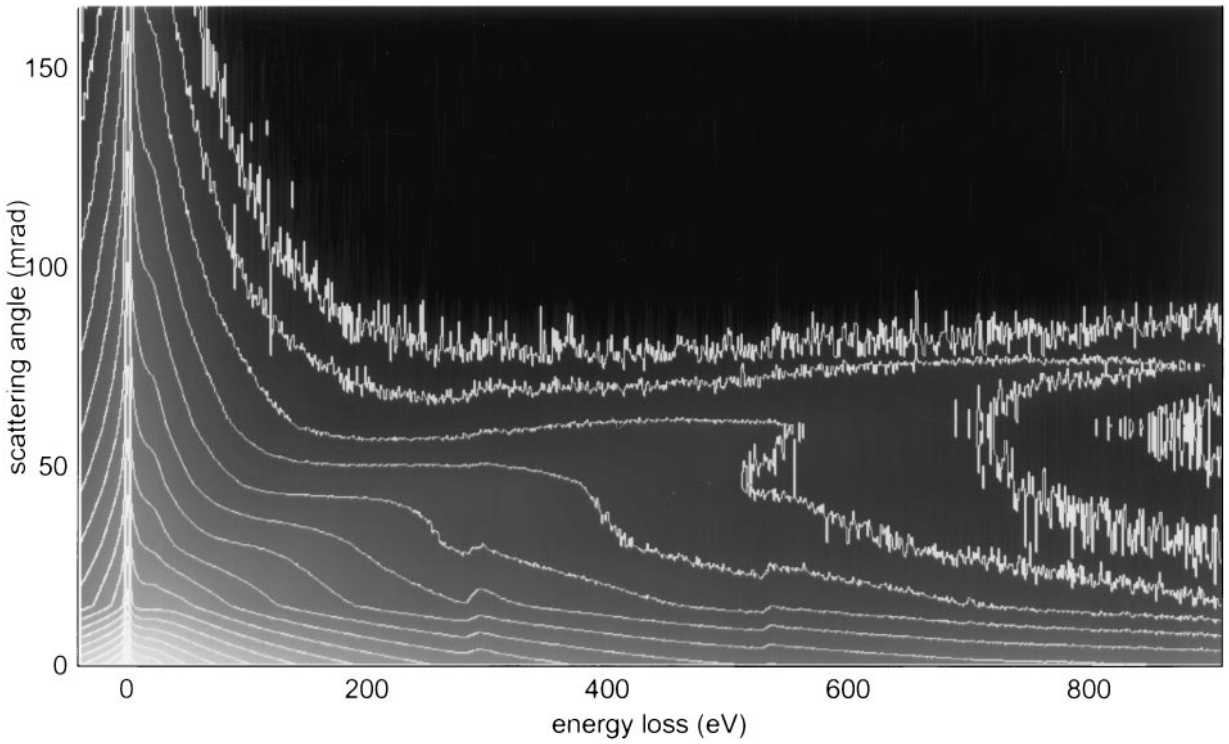

Fig. 1. Experimentally measured scattered intensity as a function of energy loss and scattering angle for a thin amorphous Ge film. The brightness is proportional to the log of the scattered intensity and in addition two contours are plotted per order of magnitude increase in scattered intensity. The measurements were made by collecting energy-loss spectra at increasing scattering angle with no deconvolution of the detector point spread and hence some intensity is visible at negative energy loss.

produces energy losses of the order of only 1/40 eV (at room temperature) but large scattering angles, and so is also found in the zero-loss peak (I will call this phonon scattering, although often the terms phonon scattering and thermal diffuse scattering are used synonymously). Higher energy losses include plasmon, single electron and core losses, whose scattering is confined mostly to small angles, and Compton scattering, which produces the parabolic shaped diffuse intensity visible at high energy loss and high scattering angles. As the specimen thickness is increased, multiple scattering becomes more important. The effect of these forms of scattering on high-resolution images will be discussed in later sections.

A typical 400-kV high-resolution microscope with a resolution of 0·15 nm resolves electrons scattered to about 10 mrad, and so the only electrons that can contribute to the *contrast* in a high-resolution image are those scattered to angles in a thin band along the very bottom of Fig. 1. All other electrons that are not excluded by apertures contribute a background of varying degree of uniformity. Any electrons that do not reach the final image because of apertures limiting the scattering angle transferred or energy filtering are effectively 'absorbed', thus reducing the overall intensity of the image.

Atomic scattering factors

The first part of any image simulation is the determination of atomic scattering factors from which the projected potential is derived. Scattering factors are the scattering from an isolated neutral atom. For most image simulations the scattering factors come from Doyle & Turner (1968) and are parameterized directly as the sum of four Gaussians. It should be remembered that these parameterized fits are only valid up to $20\,\mathrm{nm}^{-1}$ (a scattering angle of 33 mrad at 400 kV) and underestimate the actual scattering at angles greater than this (see Fig. 2), although Weickenmeier & Kohl (1991) have used a different method of fitting which gives better fits at high scattering angle. In fact, a much better fit is obtained at high angles using parameterized X-ray scattering factors and the Mott formula (although for some elements where the constant term in the X-ray scattering factor fitting parameters is large X-ray parameters are also poor), or for very high angles the simple Rutherford scattering formula. Unfortunately, at low scattering angles the Mott formula becomes increasingly inaccurate. More recently, Rez *et al.* (1994) have recalculated the atomic scattering factors and obtained results that are very similar to those of Doyle & Turner (1968). Thus the

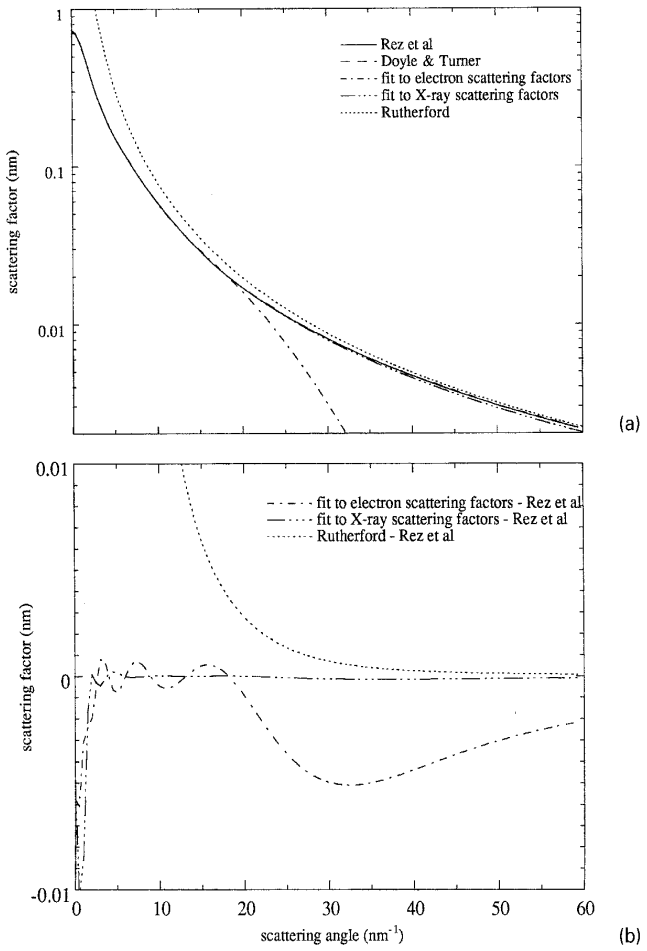

Fig. 2. (a) Atomic scattering factor for As plotted on a log scale. The lines from Rez *et al.* (1994) and Doyle & Turner (1968) are the actual values as tabulated in the papers up to 60 nm^{-1}. The fits to the electron and X-ray scattering factors are the standard parameterized four Gaussian fits to the tabulated electron and X-ray scattering factors, subsequently converted to an electron scattering factor using the Mott formula for the X-ray case, and are valid only over the range of the fit, i.e. up to 20 nm^{-1}. The final line is from the Rutherford scattering formula, $f_e = m_e e^2 Z/2h^2 s^2$. (b) Difference between the atomic scattering factors plotted in (a) and those calculated by Rez *et al.* (1994) (solid line in a), plotted on a linear scale.

greatest errors in scattering factors themselves come not from whose scattering factors are used but from the method of parameterization. This seems unnecessary, as with modern computers it is just as easy to store the complete scattering factor table and interpolate for intermediate values and use the Rutherford formula for values beyond the calculated values.

Conveniently, for high-resolution images of simple structures the scattering angles used fall in the intermediate range, e.g. for GaAs from 3·06 nm^{-1} (5·0 mrad at 400 kV) for 111 to 7·07 nm^{-1} (11·6 mrad) for 400 at the upper limit of most microscopes' resolution. Problems are likely to occur for calculations involving high scattering angles, e.g. of high-order Laue zone intensities (the first-order Laue zone for GaAs at 400 kV is at 55·1 nm^{-1} or 90·5 mrad) or high-angle dark-field intensities and for very small scattering angles, such as in complex structures with very large unit cells, interface problems where large supercells need to be used or calculations of Fresnel contrast. In reality account should also be taken of the effects of chemical bonding. For ionic materials, scattering factors are provided which differ from neutral scattering factors only at small scattering angles, but in practice most ionic materials are only partly ionized (e.g. Anstis *et al.*, 1973). Recent investigations (Stobbs & Stobbs, 1995; Gemming, 1998) have concluded that, at least for Al_2O_3, neutral scattering factors are a better approximation for some ionic materials. Given that the contrast in an experimental high-resolution image of a simple neutral material such as Si is still much lower than in simulations, scattering factors alone cannot account for the problem.

Bonding and diffraction pattern matching

Here, rather than compare image intensities we go back a stage in image formation and compare the diffracted beam intensities, and thus avoid having to consider the imaging properties of the objective lens. Chemical bonding, whether ionic or otherwise, will alter the electron distribution around each atom and will in turn affect the amplitudes of the diffracted beams, mainly for small scattering angles. This is most easily measured by convergent beam diffraction, although attempts have been made to match high-resolution images taking account of bonding (e.g. Hiratsuka, 1991). Convergent beam measures beam intensities vs. scattering angle at constant specimen thickness and has been used both on a systematic row (Zuo & Spence, 1991) and at a zone axis (Bird & Saunders, 1992; Midgley & Saunders, 1996) to measure the changes in scattering caused by the rearrangement of electrons between the atoms as a result of chemical bonding in materials such as Si (Saunders *et al.*, 1995). They have been able to match the beam intensities to within a fraction of a per cent and obtain agreement to this level with similar measurements made by X-ray diffraction. Even before refining the structure factors the neutral atom structure factors agree with experiment to within a few per cent. This might suggest that calculations of the intensities of the diffracted beams are accurate and the problem for high-resolution images lies with the calculation of the effect of the objective lens. However, there are a few complications—although the experimental convergent beam patterns are energy filtered, the effects of phonon scattering have to be removed and typically this is done by fitting and subtracting a constant background from each convergent beam disc whose value may be about 5% of

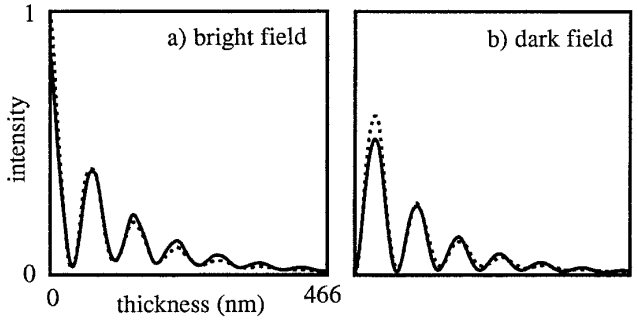

Fig. 3. (a) Bright-field and (b) dark-field energy-filtered thickness fringes measured experimentally (solid line) and calculated (dotted line) for GaAs at a temperature of 93 K, using 400-kV electrons and an objective aperture radius of 2·06 mrad (Dunin-Borkowski *et al.*, 1995).

the total disc intensity. Also, high-resolution images are obtained from very thin crystals whilst convergent beam patterns are typically obtained from very thick parts of the specimen where the effects of the surfaces and amorphous layers (see later) are minimized.

Thickness fringes

Thickness fringes provide another way of comparing experimental and simulated beam intensities by measuring the intensity of each beam as a function of specimen thickness in the appropriate two-beam bright-field or dark-field image. In this case we are measuring the beam intensity as a function of specimen thickness at constant angle of incidence. Such comparisons were first done many years ago (e.g. Watanabe *et al.*, 1962; Metherell, 1967) from which absorption parameters were found, and an example is shown in Fig. 3 for GaAs (Dunin-Borkowski *et al.*, 1995). It is possible to adjust V_g (the Fourier coefficient of the lattice potential in volts) and the Debye–Waller factor to match the extinction period then fit V_0' and V_g' (the imaginary, and thus absorptive, parts of the Fourier representation of the lattice potential) to get the amplitudes right. This can be done for both filtered and unfiltered images resulting in different V_0' and V_g' values. Generally, the fit is much poorer than for convergent beam matching as described above, with the worst fit being at low thicknesses where the first bright fringe in dark field is usually stronger in the simulations than is found experimentally. This is just the range of thickness at which high-resolution images are taken, and the extra intensity in the first dark-field thickness fringe in simulated thickness fringes agrees with the extra contrast found in simulated high-resolution images. In addition, any effects due to surfaces are more likely to show at low thickness. Even though the calculated intensities are worst at low thickness, the disagreement is generally small (e.g. the first dark thickness fringe is only about 20% brighter in the GaAs simulation of Fig. 3b), and nowhere near the factor of three needed to explain fully the low contrast in high-resolution images.

Phonon and thermal diffuse scattering

Phonon scattering involves losses of less than 0·1 eV and so cannot be removed by energy filtering. Electrons suffering phonon scattering are scattered through comparatively large angles, unlike for plasmon scattering, and so can be considered to a first approximation to add a constant background to high-resolution images, thus reducing their contrast without significantly changing their pattern. It is for this reason that absorption coefficients must be used carefully in high-resolution simulations. They have generally been determined from (or for) bright-field or dark-field images with small objective apertures where most of the phonon scattering is prevented from reaching the image by the objective aperture. In a high-resolution image simulation such absorption coefficients would correctly estimate the diffracted beam intensities but underestimate the amount of background scattering contributing, owing to the much larger objective aperture used. It should also be remembered for unfiltered images that not all the diffuse scattering between the diffraction discs is phonon/thermal diffuse (Eaglesham & Berger, 1994).

The main contribution of phonon and thermal diffuse scattering to the pattern of images is in high-angle annular dark field, where for the typical scattering angles used they make a significant, if not a majority, contribution to the image contrast (Wang & Cowley, 1989; Boothroyd *et al.*, 1995; Wang & Li, 1995; Hartel *et al.*, 1996). A number of people have made calculations of the contribution of phonon scattered electrons to high-resolution images (e.g. Möbus *et al.*, 1996). Wang (1992) concluded that for a small spherical aberration coefficient, imaging of phonon scattered electrons was incoherent and that phase coupling between adjacent atoms would not affect high-resolution images, only diffraction patterns, allowing relatively simple simulations based on the Einstein model to be used for images.

The degree to which phonon scattering affects high-resolution image contrast can be estimated from the intensity remaining between the discs of an energy-filtered convergent beam pattern. In most cases this is small compared with the number of electrons in the convergent beam discs themselves for the thicknesses used in high resolution, although this may be less true if no objective aperture is used.

Inelastic scattering

It has for a while been suggested that inelastically scattered electrons can contribute contrast to high-resolution images

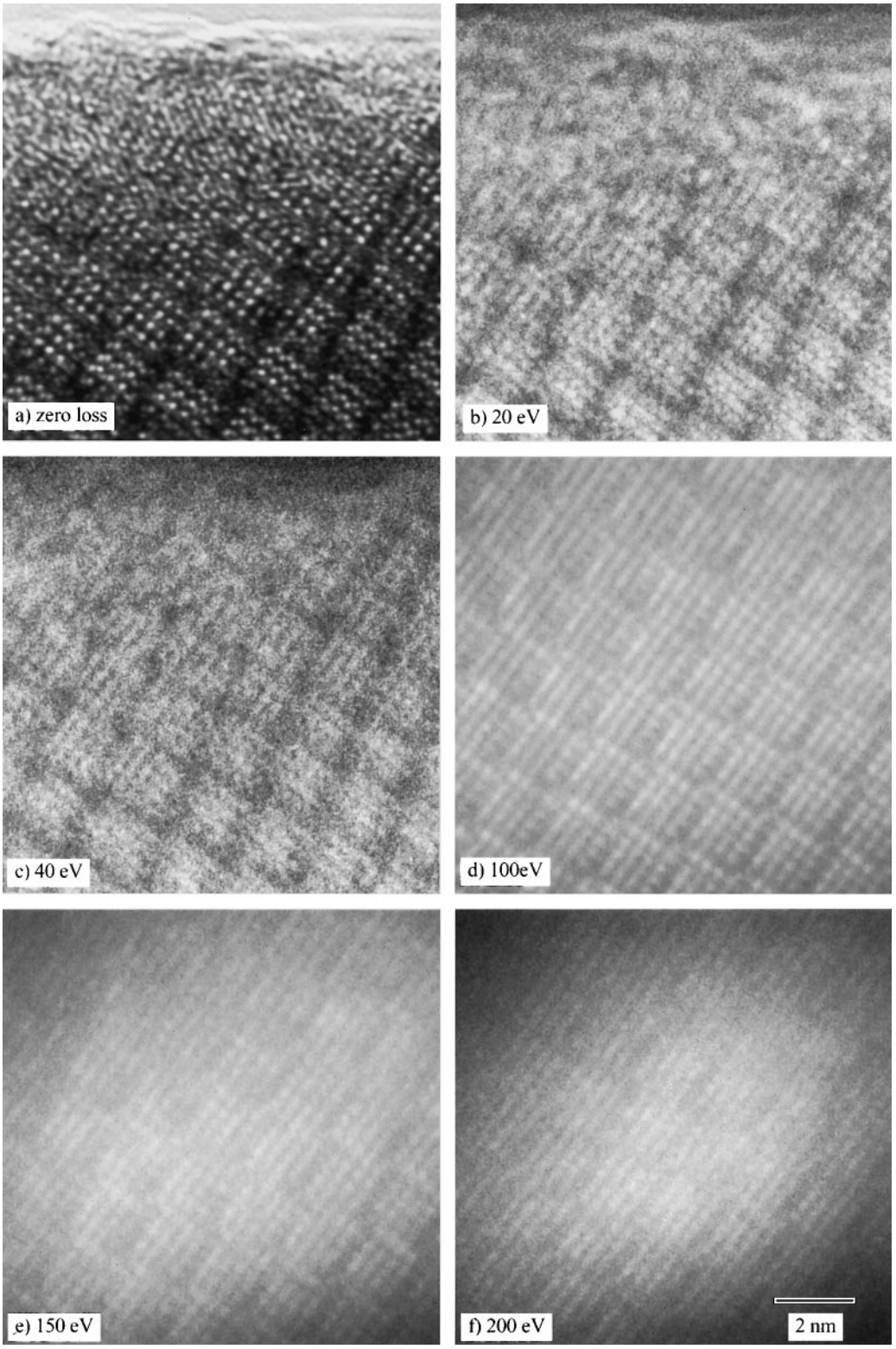

Fig. 4. Experimental filtered images of $8WO_3 9Nb_2O_5$ taken at 200 kV on a Philips CM200 FEG as a function of energy loss. For the loss images the microscope voltage was raised, keeping the energy filter magnet current unchanged so that the electrons of the energy loss being imaged remained in focus. (a), (b) and (c) are from approximately the same specimen area and with the same illumination conditions whilst for (d), (e) and (f) a focused probe was needed to get enough intensity in the loss image.

(Boothroyd & Stobbs, 1988; Stobbs & Saxton, 1988; Boothroyd & Stobbs, 1989). Figure 4 shows energy-filtered images of $8WO_3 9Nb_2O_5$ taken as a function of energy loss (and see also those of Hashimoto, 1996; Hashimoto *et al.*, 1996). The energy-loss images were obtained by raising the microscope voltage by an amount equal to the energy loss being imaged, ensuring that the focusing by the objective and subsequent lenses is identical for each image and thus that each image is in focus. Such an image series demonstrates that energy-loss electrons can be imaged at atomic resolution even though the initial energy loss process is incoherent, owing to their 'subsequent' elastic scattering. It is not obvious what specimen thickness to use in simulations of such images, as quantum mechanically we cannot determine the order of scattering.

When considering the inelastic contributions to an unfiltered lattice image, account has to be taken of the chromatic aberration of the objective lens in imaging electrons that have lost energy at a greater overfocus than the zero-loss electrons. Figure 5 shows unfiltered, zero-loss, first and second plasmon loss filtered images taken by changing the voltage on the spectrometer drift tube, from which it can be seen that the loss images are overfocus with respect to the zero-loss image. This means that when the zero-loss image is near to Scherzer defocus, the plasmon-loss images are overfocus, and thus the plasmon-loss electrons will have the greatest contribution to the pattern of unfiltered images taken at larger underfocus.

The contributions of loss electrons to image contrast for $8WO_3 9Nb_2O_5$ have been investigated by Boothroyd *et al.* (1995). They found that even for the thinnest regions near the specimen edge (10 nm) about 15% of the electrons reaching the image had been inelastically scattered. Despite this large inelastic contribution, the pattern of the unfiltered and filtered images was very similar even though the contrast in the unfiltered images was reduced by a factor of about two when compared with the filtered images. Even when energy-filtered images were compared with simulations the contrast in the experimental images was still about a factor of three lower than in the simulations. Thus, although inelastic scattering does affect the image contrast, it is not enough on its own to explain the low contrast in high-resolution images.

Amorphous layers

Most real specimens come complete with an amorphous surface layer, either from the specimen thinning process (e.g. ion milling) or due to carbon contamination in the microscope. The most obvious effect of such layers is the addition of noise to the image (Gibson & McDonald, 1987). This results from the elastic scattering by the amorphous material, whose effect is to alter the phase of the electrons without significantly reducing the amplitude. Boothroyd *et al.* (1995) have shown that if lattice averaging is used to remove the noise then the main effect of such amorphous layers is a small reduction in image contrast by the addition of a constant background. A much more significant effect is the inelastic scattering caused by the amorphous layer. For energy filtered images this just causes a reduction in the image intensity without loss of contrast, but for unfiltered images such scattering, mostly at the plasmon energy of carbon (23 eV) and with associated angular scattering, will add to the inelastic scattering from the specimen itself, resulting in an additional reduction in image contrast (Boothroyd & Stobbs, 1989; Preston, 1996).

The effect of a layer of amorphous carbon was examined experimentally by Boothroyd *et al.* (1995) by comparing images of parts of the crystal covered by and overhanging the carbon support film and it was found that carbon scattered only about 4% of the electrons elastically, but about 15% inelastically. Thus the effect of an amorphous layer on the contrast of a filtered image is small, but will be much larger for an unfiltered image.

Fringing fields

All image simulations assume the specimen potential drops to zero abruptly outside the specimen. In reality this is not true. The difference is most noticeable when charges are widely separated, as for example in a layer of one material embedded in another (such as in semiconductor heterostructures) or in a p–n junction. However, small fringing fields do extend from the atoms at the surface of a specimen. Calculations for fringing fields for layers and p–n junctions (Dunin-Borkowski & Saxton, 1997) show that most of the phase change that electrons experience happens in the fringing field outside the specimen, although the resultant phase changes are still remarkably similar to those calculated assuming all the field is contained within the specimen itself. Fringing fields are most important when the features causing them are large compared with the specimen thickness and will thus affect Fresnel imaging and high-resolution images of large unit cell ionic structures more than small unit celled covalent structures or convergent beam patterns of thick crystals.

Electron beam damage

Electron beam damage is a common problem with many specimens and can take the form of displacement of atoms from their sites or the formation of various kinds of defects. Knock-on damage leads to a gradual reduction in the image contrast as the lattice is destroyed. Often the formation of defects produces strain resulting in local crystal tilts (Walther *et al.*, 1995). However, in any quantification of high-resolution contrast, the presence of beam

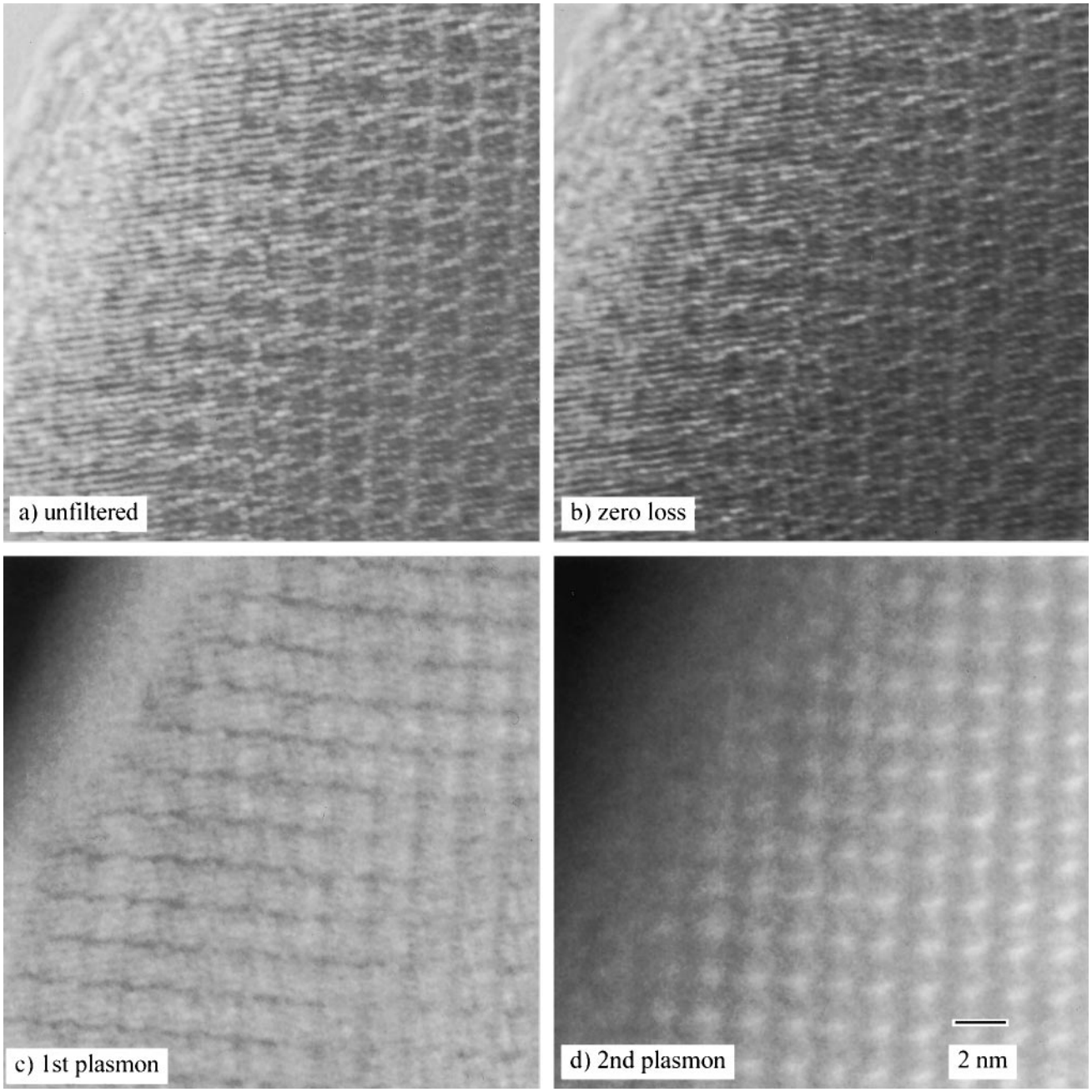

Fig. 5. Experimental unfiltered and filtered images of $8WO_3 9Nb_2O_5$ taken as above but with the microscope voltage kept constant and the spectrometer drift tube voltage adjusted to obtain the energy loss desired. The effects of chromatic aberration are seen in making the loss images more overfocus with respect to the zero-loss image.

damage can at least be demonstrated by comparing images as a function of time.

Determination of experimental parameters

This is perhaps more of a problem than it seems. Some parameters, such as microscope voltage, spherical aberration and focal spread due to instabilities, are a function of the microscope and thus need to be determined only once. Some, such as specimen thickness, are a function of the particular material and can (at least in principle) be determined in a separate experiment. Most, such as defocus, astigmatism, beam tilt, divergence and specimen vibration, are unique to a particular image or set of images. Ideally, as many

parameters as possible should be determined independently of the image series being quantified and no parameters can be considered correct until all of a long focal series (and better still a tilt series) can be matched at all thicknesses. It is impossible to obtain a believable match to one thickness at one defocus alone, especially if the crystal has a small unit cell. For example, for Si 110 imaged in a typical microscope whose resolution limit is about 0·18 nm, most of the image contrast is generated by the four 111 reflections (0·314 nm) with small contributions from 200 (0·272 nm), which is forbidden but present through double diffraction, and 220 (0·192 nm), which is just on the resolution limit. Given that the amplitudes and phases of all the 111 beams are related by symmetry and the 200s to the 111s by double diffraction this leaves only three parameters (amplitude of 000 and 111 and phase of 111 relative to 000) to describe a 110 image with a further two (amplitude and phase of 220) if the defocus is close to a passband for 220. Clearly, if the imaging parameters are not determined separately it is possible to fit such a 110 Si image quantitatively with many combinations of thickness, defocus, divergence, etc.

One of the most consistent findings is that a better match with simulations is usually found if the specimen thickness in the simulations is made much too small. This effectively produces images with low contrast which match experimental images better than the correct thickness. Hÿtch & Stobbs (1994) demonstrated this well by showing how good a fit can be obtained to a long focal series of [001] $Al_{0·3}Ga_{0·7}As$ images using about 1/8th of the independently measured specimen thickness, and King & Campbell (1993) likewise fitted [001] Nb images to simulations with a thickness of only one or two unit cells.

For the highest resolution images it should be noted that accurate matching requires very accurate determination of the microscope parameters; for example, it needs an error in defocus of only 7 nm to produce a phase shift of $\pi/2$ at a spacing of 0·15 nm at 400 kV, meaning that the defocus, astigmatism and three-fold astigmatism must be determined to within about 2 nm. Similarly, misalignment of the crystal to give a small tilt away from the zone axis has been suggested by O'Keefe & Radmilovic (1994) as a cause for reduced contrast in experimental high-resolution images. Specimen vibration cannot be the cause of the low experimental contrast alone, as it reduces the amplitude of high frequencies mostly, whereas in practice the low frequencies are also present at too low an amplitude (Boothroyd *et al.*, 1995).

The use of a largish objective aperture can be of help in putting a known limit on the beams actually contributing to the image and in reducing any high-angle elastic and phonon scattering and stray inelastic scattering contributions. However, considerable care has to be taken that the aperture is clean. Any charging round the edge of the aperture will produce unpredictable amounts of astigmatism and three-fold astigmatism.

Stray scattering

Any source of stray scattering will lead to the addition of a constant background and thus a reduction in image contrast. Possible sources are high-angle and/or high-energy-loss electrons scattered by the specimen and X-rays generated in the camera chamber from electrons passing through the film. For Gatan energy filters another source is electrons striking the drift tube. Most such stray electrons can be eliminated or at least tested for by comparing image intensities with and without the objective, selected area or spectrometer entrance apertures.

Detector point spread function

All image recording systems (film, CCD, imaging plates) suffer some form of point spread function, where intensity spreads into neighbouring pixels. For CCD detectors as used in imaging filters, the biggest cause of spreading is the channelling of light in the scintillator which leads to very wide tails on the point spread function and thus a comparatively large (typically to 2/3 of the original value) loss of contrast even at low frequencies. Methods for determining the point spread function have recently been discussed by Zuo (1996), the two most popular methods being the 'noise' method and the 'edge' method, but it is very difficult to determine the point spread function accurately. Although the point spread function of the scintillator is circularly symmetric, it is sampled on the square grid of the CCD pixels so that the resulting modulation transfer function is *not* circularly symmetric. It is therefore not possible to use radial averaging of the modulation transfer function to remove noise; doing so usually results in a spurious kink at the Nyquist frequency. Examples of modulation transfer functions for the diagonal direction for three CCD detectors are shown in Fig. 6. An image uncorrected for the detector point spread function can have a large reduction in image contrast, as can be seen from Fig. 6, but for a typical image where the lattice fringes have a wavelength of 10 pixels the detector point spread still only reduces the contrast to around 2/3 of its original value.

Conclusion

None of the above contrast reducing mechanisms is enough on its own to account for the typical factor of three difference in contrast between experimental and simulated high-resolution images. To get a better idea of what is going on, more careful quantitative comparisons of experimental images and simulations are needed, which is actually rather difficult. A long focal series is required as a function of thickness, with all the experimental parameters determined independently, of a crystal with a large unit cell to enable the comparison of the transfer of many spatial frequencies.

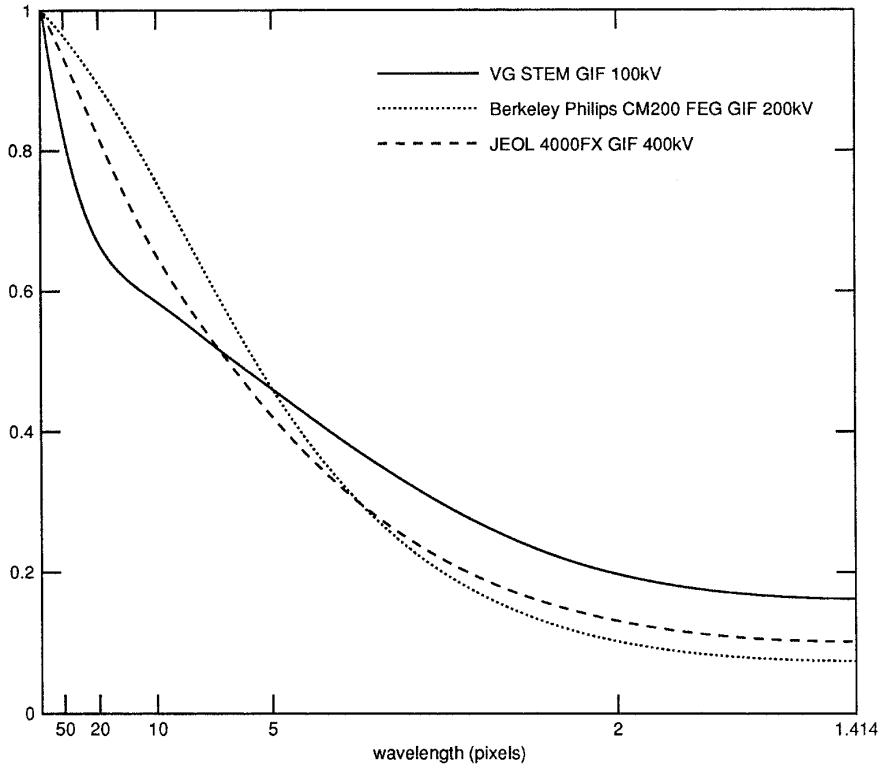

Fig. 6. Modulation transfer functions for the diagonal direction of three CCD detectors on different Gatan imaging filters determined by the noise method.

No material is ideal, but possibilities include cleaved wedges of semiconductors (known thickness, well-known structure and clean surfaces but too small a unit cell), MgO (or similar material) smoke cubes (known thickness, but may damage under the beam and still a small unit cell) or complex oxides (such as $8WO_3 9Nb_2O_5$ (Roth & Wadsley, 1965), which have large unit cells but whose thickness is difficult to determine and whose structure may be less well known). The good match of diffraction patterns and slightly less good match of thickness fringes both suggest that the problem lies more in the imaging by the objective lens part of the calculation rather than the calculation of the beam intensities. I suspect that the solution will turn out to be a combination of many factors rather than just one of the above.

Acknowledgments

I would like to thank Dr C. J. D. Hetherington and the Lawrence Berkeley National Laboratory for the use of their facilities, Dr R. E. Dunin-Borkowski and Dr A. R. Preston for their considerable help and the late Dr W. M. Stobbs for the inspiration behind this work.

References

Anstis, G.R., Lynch, D.F., Moodie, A.F. & O'Keefe, M.A. (1973) *n*-beam lattice images. III. Upper limits of ionicity in $W_4Nb_{26}O_{77}$. *Acta Crystallogr. A*, **29**, 138–147.

Bahr, G.F. & Zeitler, E.H. (1965) *Quantitative Electron Microscopy*. Williams and Wilkins, Maryland.

Bird, D.M. & Saunders, M. (1992) Sensitivity and accuracy of CBED pattern-matching. *Ultramicroscopy*, **45**, 241–251.

Boothroyd, C.B., Dunin-Borkowski, R.E., Stobbs, W.M. & Humphreys, C.J. (1995) Quantifying the effects of amorphous layers on image contrast using energy filtered transmission electron microscopy. *MRS Symposium Proceedings*, Vol. 354 (ed. by D. C. Jacobson, D. E. Luzzi, T. F. Heinz and M. Iwaki), pp. 495–500. Materials Research Society, Pittsburgh.

Boothroyd, C.B., Dunin-Borkowski, R.E. & Walther, T. (1997) The scattering distribution from semiconductors as a function of angle and energy loss in the electron microscope. *Atomic Resolution Microscopy of Surfaces and Interfaces. MRS Symposium Proceedings*, Vol. 466 (ed. by D. J. Smith), pp. 113–118. Materials Research Society, Pittsburgh.

Boothroyd, C.B. & Stobbs, W.M. (1988) The contribution of inelastically scattered electrons to high resolution images of (Al,Ga) As/GaAs heterostructures. *Ultramicroscopy*, **26**, 361–376.

Boothroyd, C.B. & Stobbs, W.M. (1989) The contribution of inelastically scattered electrons to [110] high resolution images of GaAs/AlAs heterostructures. *Ultramicroscopy*, **31**, 259–274.

Campbell, G.H. (1996) Σ5 (210) /[001] symmetric tilt grain boundary in yttrium aluminium garnet. *J. Am. Ceram. Soc.* **79**, 2883–2891.

Cherns, D., Anstis, G.R., Hutchinson, J.L. & Spence, J.C.H. (1982) The atomic structure of the $NiSi_2$/(111) Si interface. *Philos. Mag. A*, **46**, 849–862.

Doyle, P.A. & Turner, P.S. (1968) Relativistic Hartree–Fock X-ray and electron scattering factors. *Acta Crystallogr. A*, **24**, 390–397.

Dunin-Borkowski, R.E. & Saxton, W.O. (1997) The electrostatic contribution to the forward scattering potential at a space charge layer in high energy electron diffraction. II. Fringing fields. *Acta Crystallogr. A*, **53,** 242–250.

Dunin-Borkowski, R.E., Schäublin, R.E., Walther, T., Boothroyd, C.B., Preston, A.R. & Stobbs, W.M. (1995) The determination of absorption parameters in Si and GaAs using energy-filtered imaging. *Electron Microscopy and Analysis 1995*, Vol. 147 (ed. by D. Cherns), pp. 179–182. Institute of Physics Publishing, Bristol.

Eaglesham, D.J. & Berger, S.D. (1994) Energy-filtering the thermal diffuse background in electron-diffraction. *Ultramicroscopy*, **53,** 319–324.

Gemming, T., Möbus, G., Exner, M., Ernst, F & Rühle, M. (1998) *Ab-initio* HRTEM simulations of ionic crystals: a case study of sapphire. *J. Microsc.* **190,** 89–98.

Gibson, J.M. & McDonald, M.L. (1987) Improving the signal-to-noise limits in high resolution transmission electron microscopy. *MRS Symposium Proceedings*, Vol. 82 (ed. by R. W. Siegel, J. R. Weertman and R. Sinclair), pp. 109–113. Materials Research Society, Pittsburgh.

Hartel, P., Dinges, C. & Rose, H. (1996) Simulation of high-angle annular dark-field images considering elastic scattering and phonon excitations. *Proc. XI European Congress on Microscopy, Dublin, 26–30 August 1996*. EUREM 96, UCD, Dublin.

Hashimoto, H. (1996) Images and diffraction patterns of lined atomic column formed by Ca-$L_{2,3}$ shell loss electron. *Proc. XI European Congress on Microscopy, Dublin, 26–30 August 1996*. EUREM 96, UCD, Dublin.

Hashimoto, H., Makita, Y. & Endoh, H. (1996) Characterisation of thin-film materials by 400 kV electron-microscope images and with an energy filter. *Mater. Chem. Phys.* **46,** 7–14.

Hiratsuka, K. (1991) Screening effect on <110> high-resolution electron microscopy image of compound semiconductors. *Philos. Mag. B*, **63,** 1087–1100.

von Hochmeister, K. & Phillipp, F. (1996) Quantitative comparison of HREM images with image simulations. *Proc. XI European Congress on Microscopy, Dublin, 26–30 August 1996*. EUREM 96, UCD, Dublin.

Hÿtch, M.J. & Stobbs, W.M. (1988) The effects of single electron and plasmon scattering on (100) and (010) images of $YBa_2Cu_3O_{7-\delta}$. *Institute of Physics Conference Series No. 93*, pp. 347–349. Institute of Physics, Bristol.

Hÿtch, M.J. & Stobbs, W.M. (1994) Quantitative comparison of high resolution TEM images with image simulations. *Ultramicroscopy*, **53,** 191–203.

Inkson, B.J. & Humphreys, C.J. (1995) High-resolution electron microscopy observation of a 1/2[112] superdislocation in TiAl. *Philos. Mag. Lett.* **71,** 307–312.

King, W.E. & Campbell, G.H. (1993) Determination of thickness and defocus by quantitative comparison of experimental and simulated high-resolution images. *Ultramicroscopy*, **51,** 128–135.

Metherell, A.J.F. (1967) Measurement of absorption of fast electrons in single crystal films of aluminium. *Philos. Mag.* **15,** 755–762.

Midgley, P.A. & Saunders, M. (1996) Quantitative electron diffraction: from atoms to bonds. *Contemp. Phys.* **37,** 441–456.

Möbus, G., Gemming, T., Gumbsch, P. & Rhüle, M. (1996) A molecular dynamics approach to thermal diffuse scattering in quantitative HREM. *Proc. XI European Congress on Microscopy, Dublin, 26–30 August 1996*. EUREM 96, UCD, Dublin.

O'Keefe, M.A. & Radmilovic, V. (1994) Specimen thickness is wrong in similated HRTEM images. *Proceedings of the 13th International Congress on Electron Microscopy* (ed. by B. Jouffrey and C. Colliex), pp. 361–362. Les Éditions de Physique, Les Ulis.

Preston, A.R. (1996) What is the difference between a dislocation crossing a bend contour and a bend contour crossing a dislocation? *Proc. XI European Congress on Microscopy, Dublin, 26–30 August 1996*. EUREM 96, UCD, Dublin.

Rez, D., Rez, P. & Grant, I. (1994) Dirac–Fock calculations of X-ray scattering factors and contributions to the mean inner potential for electron scattering. *Acta Crystallogr. A*, **50,** 481–497.

Roth, R.S. & Wadsley, A.D. (1965) Multiple phase formation in the binary sytem Nb_2O_5–WO_3 III. The structures of the tetragonal phases $W_3Nb_{14}O_{44}$ and $W_8Nb_{18}O_{69}$. *Acta Crystallogr.* **19,** 38.

Saunders, M., Bird, D.M., Zaluzec, N.J., Burgess, W.G., Preston, A.R. & Humphreys, C.J. (1995) Measurement of low-order structure factors for silicon from zone-axis CBED patterns. *Ultramicroscopy*, **60,** 311–323.

Stobbs, W.M. & Saxton, W.O. (1988) Quantitative high resolution transmission electron microscopy: the need for energy filtering and the advantages of energy-loss imaging. *J. Microsc.* **151,** 171–184.

Stobbs, W.M. & Stobbs, S.H. (1995) Can the ionicity of sapphire be determined using HREM? *Electron Microscopy and Analysis 1995*, Vol. 147 (ed. by D. Cherns), pp. 83–86. Institute of Physics, Bristol.

Walther, T., Boothroyd, C.B. & Humphreys, C.J. (1995) Strain relaxation induced local crystal tilts at Si/SiGe interfaces in cross-sectional transmission electron microscope specimens. *Microscopy of Semiconducting Materials 1995*, Vol. 146 (ed. by A. G. Cullis and A. E. Staton-Bevan), pp. 11–16. Institute of Physics, Bristol.

Wang, Z.L. (1992) Dynamics of thermal diffuse scatering in high-energy electron diffraction and imaging: theory and experiments. *Philos. Mag. B*, **65,** 559–587.

Wang, Z.L. & Cowley, J.M. (1989) Simulating high-angle annular dark-field STEM images incuding inelastic thermal diffuse scattering. *Ultramicroscopy*, **31,** 437–454.

Wang, Z.L. & Li, D.C. (1995) Dynamical diffraction of double-inelastically scattered electrons. *Philos. Mag. B*, **71,** 201–219.

Watanabe, H., Fukuhara, A. & Kohra, K. (1962) Measurement of mean and anomalous absorption coefficients of electrons in MgO crystals by the use of electron micrographic images. *J. Phys. Soc. Jpn*, **17,** 195–199.

Weickenmeier, A. & Kohl, H. (1991) Computation of absorptive form factors for high energy electron diffraction. *Acta Crystallogr.* **A47,** 590–597.

Zuo, J.M. (1996) Electron detection characteristics of slow-scan CCD camera. *Ultramicroscopy*, **66,** 21–33.

Zuo, J.M. & Spence, J.C.H. (1991) Automated structure factor refinement from convergent-beam patterns. *Ultramicroscopy*, **35,** 185–196.